Electronic Structure of f^1 Actinide Complexes. 1. Nonrelativistic and Relativistic Calculations of the Optical Transition Energies of AnX_6^{q-} Complexes

Nikolas Kaltsoyannis[1] and Bruce E. Bursten*

Department of Chemistry, The Ohio State University, Columbus, Ohio 43210

Received February 24, 1995[⊗]

The ground-state electronic structures of PaX_6^{2-} (X = F, Cl, Br, I), UX_6^- (X = F, Cl, Br), and NpF_6 have been calculated, using both nonrelativistic and relativistic implementations of the discrete-variational Xα (DV–Xα) method. A significant amount of metal–ligand covalent bonding is found, involving both 6d and 5f metal orbitals. The 5f contribution to the bonding levels increases significantly from PaX_6^{2-} to UX_6^- to NpF_6 but remains approximately constant as the halogen is altered in PaX_6^{2-} and UX_6^-. In contrast, the 6d atomic orbital character of the halogen-based levels increases from UF_6^- to UBr_6^- and a similar, though less marked, trend is observed in PaX_6^{2-}. The electronic transition energies have been calculated using the transition state method. The relativistic calculations are far superior to the nonrelativistic ones in both qualitatively and quantitatively describing the electronic spectra. The stabilization of the metal 5f atomic orbitals with respect to the halogen *n*p levels from protactinium to neptunium results in the more energetic f → f transitions in NpF_6 being masked by the onset of a ligand-to-metal charge-transfer band. In the remaining molecules, the f → f transitions occur well removed from charge-transfer bands.

Introduction

The factors that dominate the electronic transition energies of complexes of the d- and f-block metals are very dependent on the position of the metal atom in the periodic table. For complexes of the first-row transition metals, the electronic transition energies are dominated by the interactions of the metal 3d orbitals with the ligand field; the effects of spin–orbit coupling can, to a good approximation, be neglected. For the lanthanide metals, the opposite is the case: Spin–orbit coupling is significant, and the highly contracted 4f orbitals are largely unperturbed by the ligand environment. Complexes of the heavier transition metals and of the actinide elements are subject to both ligand-field and spin–orbit effects. The 5f atomic orbitals of the early actinide elements, which will be the focus of this paper, have significantly greater radial extension and are subject to much greater spin–orbit coupling than are the 4f AOs of the lanthanides.

The calculation of optical transition energies is one of the greatest challenges of electronic structure theory. Electronic structure calculations are easiest for closed-shell molecules, but the calculation of optical transition energies necessarily involves open-shell configurations (in either or both the ground and excited states). The situation is further exacerbated in actinide-containing molecules for a number of reasons.[2,3] Aside from the intrinsic difficulty associated with the calculation of the electronic structure of these many-electron, heavy-element systems, the large number of orbitals on actinide centers generally leads to a large number of closely spaced ligand-field transitions that can be difficult to assign.

The discrete-variational Xα (DV–Xα) density functional method of Ellis[4] is now firmly established as a powerful tool in electronic structure determination. We have applied both nonrelativistic and fully relativistic implementations of this approach to a number of actinide-containing systems.[5,6] Success in this area has prompted us to embark on a project to calculate the optical transition energies of a wide range of actinide complexes, with examples drawn from the realms of classical coordination and organometallic chemistry.

In order to minimize the problems associated with multiple-electron configurations, we have focused first on complexes that contain only one metal-localized electron. Numerous actinide complexes contain the metal atom in a formal oxidation state 1 less than its group valence. Examples of these "f^1" complexes include the tetrahedral borohydride compounds $[Pa(BH_4)_4]$ and $[Pa(BH_3CH_3)_4]$,[7] organometallic systems such as $[Th(\eta^5\text{-}C_5H_3(SiMe_3)_2)_3]$,[8] $[Pa(\eta^8\text{-}C_8H_8)_2]$,[9] and $[U(\eta^5\text{-}C_5H_5)_3NPh]$,[10] and of course the isoelectronic octahedral hexahalide complexes PaX_6^{2-} (X = F, Cl, Br, I), UX_6^- (X = F, Cl, Br), and NpF_6. We have elected to begin with these latter molecules, a choice that provides compounds that are chemically familiar and whose high symmetry simplifies the interpretation of calculational results. Further, these compounds have already received substantial experimental and theoretical study, which gives us the opportunity to test our methodology before addressing the more complex systems listed above.

Methodology and Computational Details

It has long been recognized that is is necessary to incorporate relativistic corrections into the molecular Hamiltonian for heavy-element systems,[11–13] and this is especially so when quantitative agreement

[⊗] Abstract published in *Advance ACS Abstracts,* April 15, 1995.

(1) Present address: Department of Chemistry, University College London, 20 Gordon Street, London WC1H 0AJ, U.K.

(2) *Lanthanide and Actinide Chemistry and Spectroscopy*; Edelstein, N. M., Ed.; American Chemical Society: Washington, DC, 1980.

(3) Pepper, M.; Bursten, B. E. *Chem. Rev.* **1991**, *91*, 719.

(4) Ellis, D. E. *J. Phys. B: Atom. Molec. Phys.* **1977**, *10*, 1.

(5) Schneider, W. F. Ph.D. Dissertation, The Ohio State University, 1991.

(6) Schneider, W. F.; Strittmatter, R. J.; Bursten, B. E.; Ellis, D. E. In *Density Functional Methods in Chemistry*; Labanowski, J. K., Andzelm, J. W., Eds.; Springer-Verlag: New York, 1991; Chapter 16.

(7) Kot, W. K. Ph.D. Dissertation, University of California, Berkeley, CA, 1991.

(8) Blake, P. C.; Lappert, M. F.; Atwood, J. L.; Zhang, J. *J. Chem. Soc., Chem. Commun.* **1986**, 1148.

(9) Starks, D. F.; Parsons, T. C.; Streitwieser, A.; Edelstein, N. M. *Inorg. Chem.* **1974**, *13*, 1307.

(10) Brennan, J. G.; Andersen, R. A. *J. Am. Chem. Soc.* **1985**, *107*, 514.

(11) Pitzer, K. S. *Acc. Chem. Res.* **1979**, *8*, 271.

(12) Pyykkö, P. *Acc. Chem. Res.* **1979**, *8*, 276.

0020-1669/95/1334-2735$09.00/0

between experiment and theory is sought. The details of our relativistic DV−Xα method have been given elsewhere,[5,6] and only a brief summary is provided here. The approach incorporates the Dirac operator into the traditional Hartree−Fock treatment, the molecular wave function being represented as a Slater determinant over four-component one-electron wave functions. Application of the variation principle to this antisymmetrized wave function yields the Dirac−Fock one-electron equations, analogous to the nonrelativistic case.[14,15] The Dirac−Fock equations contain both relativistic one-electron terms and nonrelativistic two-electron terms that correspond to electrostatic electron−electron repulsions. The latter terms are replaced by a Coulomb repulsion operator and an approximate local-density-functional exchange-correlation operator. The simplest choice for this operator is Slater's Xα potential,[16,17] although the improved parameterization of Hedin and Lundqvist[18] has been employed in the calculations reported here.

The molecular orbitals (MOs) are expressed in the usual linear combination of atomic orbitals (LCAO) expansion over a basis of symmetry-adapted four-component atomic functions. The large and small radial components are obtained from numerical atomic Dirac−Fock−Slater calculations, performed on neutral atoms and cations and subsequently combined to provide a "multi-ζ" basis of approximately split-valence quality.[5] The self-consistent-multipolar charge density representation is used in evaluating the molecular Coulomb integrals.[19] A Mulliken population analysis[20] is employed in order to provide an approximate estimation of the molecular charge density.

Ground state MO energy differences are often misleading, particularly when the electronic transition involves orbitals of very different character. Therefore, the familiar transition state method of Slater[17,21] is used to calculate the electronic transition energies.

All molecules were constrained to octahedral symmetry. The Np−F distance has been determined by gas-phase electron diffraction to be 1.981 Å.[22] The M−X bond lengths in the remaining complexes were estimated from Shannon's ionic radii for U^{5+} and Pa^{4+} under 6-fold coordination[23] and from Pauling's ionic radii for F^-, Cl^-, Br^-, and I^-.[24] The assumed bond lengths are 2.09 Å for U−F, 2.57 Å for U−Cl, 2.72 Å for U−Br, 2.23 Å for Pa−F, 2.71 Å for Pa−Cl, 2.86 Å for Pa−Br, and 3.10 Å for Pa−I.[25]

All calculations were performed on the Cray Y-MP/864 supercomputer at The Ohio Supercomputing Center.

Results and Discussion

The results presented here will naturally be compared to both the experimental and theoretical work that has gone before. The low-resolution gas-phase electronic absorption spectrum of NpF_6 has been reported by Eisenstein and Pryce[26] and by Steindler and Gerding.[27] Recently Mulford et al. investigated the near-infrared vibronic transitions of NpF_6 in argon matrices using absorption and fluorescence spectroscopy.[28] The absorption spectra of UX_6^- (X = F, Cl, Br) have been measured by Ryan,[29] while Edelstein and co-workers have reported those of PaX_6^{2-} (X = F, Cl, Br, I).[30−35] $PaCl_6^{2-}$ was also the subject of a more recent fluorescence spectroscopic investigation by Piehler et al.[36]

On the theoretical side, Boring et al. used the nonrelativistic Hartree−Fock−Slater method in the multiple-scattering approach to study UF_6 and UF_6^-.[37] Hay et al. used ab initio calculations with relativistic effective core potentials (RECPs) and a spin−orbit operator to investigate UF_6^+, UF_6, and UF_6^-, including the electronic transitions of the last.[38] Thornton, Rösch, and Edelstein used the quasi-relativistic Xα−SW method to investigate the electronic structure and f−f electronic transitions of all of the systems discussed here within a single-group description.[39] Case performed relativistic Dirac-scattered-wave calculations on NpF_6.[40] Koelling, Ellis, and Bartlett have investigated the ground- and excited-state electronic structure of UF_6, NpF_6, and PuF_6 by using an early implementation of the relativistic DV−Xα method employed here.[41] These latter molecules were recently revisited by Kocab[42] via an ab initio SCF method using RECPs together with a spin−orbit operator.

The results presented here involve fully relativistic calculations under the molecular double group. Nevertheless, we begin by providing a brief discussion of NpF_6, UF_6^-, and PaF_6^{2-} from a nonrelativistic standpoint under the usual O_h single group. This discussion will serve to highlight the deficiencies of nonrelativistic calculations in discussing heavy-element systems and will provide a comparison with the relativistic results. We shall then present the relativistic calculations on the ground-state systems, examining in particular some of the trends found in metal−ligand bonding as a function of both M and X. Following the presentation of the results of the ground-state calculations, we will turn to a discussion of the electronic transition energies, both predicted and found, of the actinide hexahalides.

Nonrelativistic Calculations on NpF_6, UF_6^-, and PaF_6^{2-}. The basic aspects of the electronic structure of octahedral metal complexes occupy a central position in the study of inorganic chemistry. Consequently only a brief summary is provided here. As with all electronic structure calculations, it is instructive to establish first the types of orbitals which the participating atoms bring to complex formation. The valence orbitals of fluorine are primarily the 2p AOs. In an octahedral F_6 cage, the 2pσ

(13) Pyykkö, P. *Chem. Rev.* **1988**, *88*, 563.
(14) Grant, I. P. *Adv. Phys.* **1970**, *19*, 747.
(15) Grant, I. P. *Methods in Computational Chemistry, Relativistic Effects in Atoms and Molecules*; Plenum Press: New York, 1988; Vol. 2, Chapter 1.
(16) Slater, J. C. *Phys. Rev.* **1951**, *81*, 385.
(17) Slater, J. C. *Adv. Quantum Chem.* **1972**, *6*, 1.
(18) Hedin L.; Lundqvist, B. I. *J. Phys. C.: Solid State Phys.* **1971**, *4*, 2064.
(19) Delley, B.; Ellis, D. E. *J. Chem. Phys.* **1982**, *76*, 1949.
(20) Mulliken, R. S. *J. Chem. Phys.* **1955**, *23*, 1833, 1841, 2338, 2343.
(21) Slater, J. C. *The Calculation of Molecular Orbitals*; Wiley: New York, 1979.
(22) Kimura, M.; Schomaker, V.; Smith, D.; Weinstock, B. *J. Chem. Phys.* **1968**, *48*, 4001.
(23) Shannon, R. D. *Acta Crystallogr.* **1976**, *A32*, 751.
(24) Pauling, L. *The Nature of the Chemical Bond*, 3rd ed.; Cornell University Press: Ithaca, NY, 1960.
(25) The results presented here are expected to be sensitive to the choice of M−X bond lengths. The internally consistent scheme for selecting bond lengths, based on the ionic radii, was necessary because of the lack of experimental data. We are grateful to a reviewer for pointing out that the structure of $CsUF_6$ has been reported (Rosenzweig, A.; Cromer, D. T. *Acta Crystallogr.* **1967**, *23*, 865). The experimental U−F distance, 2.057(6) Å, is close to that obtained by our scheme, 2.09 Å, which gives us confidence in our selection of bond lengths.
(26) Eisenstein, J. C.; Pryce, M. L. H. *Proc. R. Soc. London, Ser. A* **1960**, *255*, 181.
(27) Steindler, M. J.; Gerding, T. J. *Spectrochim. Acta* **1966**, *22*, 1197.
(28) Mulford, R. N.; Dewey, H. J.; Barefield, J. E. *J. Chem. Phys.* **1991**, *94*, 4790.
(29) Ryan, J. L. *J. Inorg. Nucl. Chem.* **1971**, *33*, 153.
(30) Brown, D.; Whittaker, B.; Edelstein, N. M. *Inorg. Chem.* **1974**, *13*, 1805.
(31) Edelstein, N. M.; Brown, D.; Whittaker, B. *Inorg. Chem.* **1974**, *13*, 563.
(32) Brown, D.; Lidster, P.; Whittaker, B.; Edelstein, N. M. *Inorg. Chem.* **1976**, *15*, 511.
(33) Edelstein, N.; Krupa, J. C.; Naik, R. C.; Rajnak, K.; Whittaker, B.; Brown, D. *Inorg. Chem.* **1988**, *27*, 3186.
(34) Edelstein, N.; Kot, W. K.; Krupa, J.-C. *J. Chem. Phys.* **1992**, *96*, 1.
(35) Edelstein, N. M.; Kot, W. K. *J. Alloys Comp.* **1993**, *193*, 82.
(36) Piehler, D.; Kot, W. K.; Edelstein, N. M. *J. Chem. Phys.* **1991**, *94*, 942.
(37) Boring, M.; Wood, J. H. *J. Chem. Phys.* **1974**, *63*, 638.
(38) (a) Hay, P. J.; Wadt, W. R.; Kahn, L. R.; Raffenetti, R. C.; Phillips, D. H. *J. Chem. Phys.* **1979**, *71*, 1767. (b) Kahn, L. R. *Int. J. Quantum Chem.* **1984**, *25*, 149.
(39) Thornton, G.; Rösch, N.; Edelstein, N. *Inorg. Chem.* **1980**, *19*, 1304.
(40) Case, D. A. *J. Chem. Phys.* **1985**, *83*, 5792.
(41) Koelling, D. D.; Ellis, D. E.; Bartlett, R. J. *J. Chem. Phys.* **1976**, *65*, 3331.
(42) Kocab, F. J. M.S. Thesis, The Ohio State University, 1990.

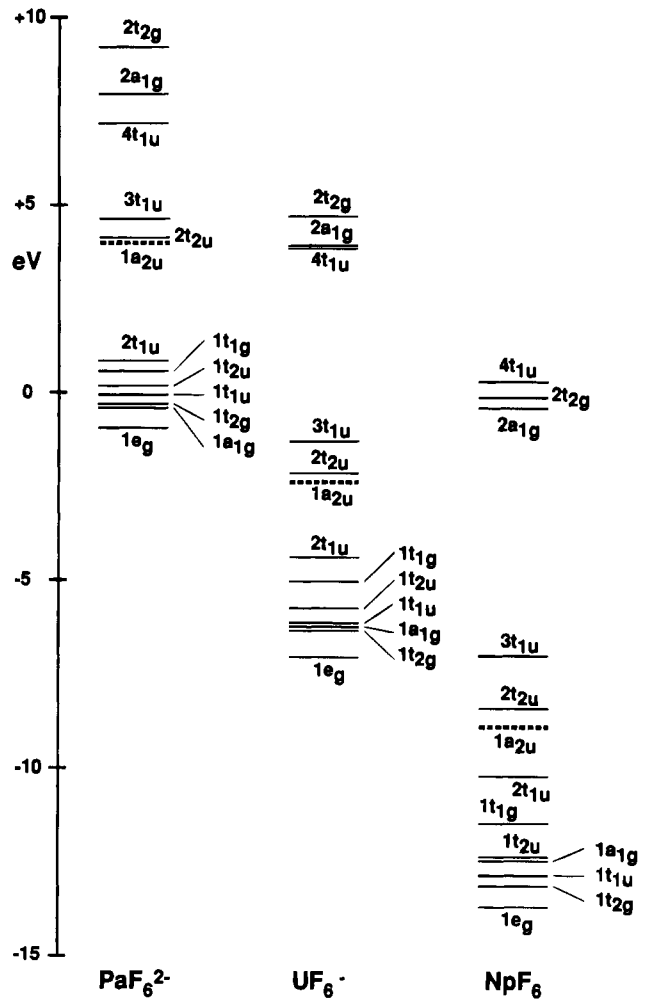

Figure 1. Molecular orbital energy level diagrams for PaF_6^{2-}, UF_6^-, and NpF_6, calculated using the nonrelativistic DV−Xα method. The highest occupied orbital is the $1a_{2u}$ level in each case and is represented by a dashed line.

orbitals (those directed at the central atom) give rise to $a_{1g} + e_g + t_{1u}$ symmetry combinations. The $2p\pi$ orbitals transform as $t_{1u} + t_{2u} + t_{1g} + t_{2g}$ in the O_h point group.

The valence AOs of the central actinide metal are the 5f, 6d, 7s, and 7p orbitals. In the nonrelativistic O_h single point group, the 7s orbitals transform as a_{1g}, the 7p as t_{1u}, the 6d as $e_g + t_{2g}$, and the 5f as $a_{2u} + t_{1u} + t_{2u}$. The a_{2u} (f_{xyz}) AO has no symmetry match with the ligand orbitals and is therefore metal−ligand nonbonding, while the t_{2u} [$f_{z(x^2-y^2)}$, $f_{x(z^2-y^2)}$, $f_{y(z^2-x^2)}$] orbitals are restricted to π-type interaction with the F_6 cage. The t_{1u} (f_{x^3}, f_{y^3}, f_{z^3}) orbitals find symmetry matches with ligand MOs derived from both fluorine $2p\sigma$ and $2p\pi$ orbitals, and consequently there is strictly no σ/π separability among the t_{1u} sets of MOs.

Figure 1 presents the MO energy levels for NpF_6, UF_6^-, and PaF_6^{2-}, calculated using the nonrelativistic DV−Xα approach. The MO energies and percent compositions for NpF_6 are provided in Table 1 and are representative of all three species.

In neutral NpF_6, the $1e_g$ through $2t_{1u}$ MOs are predominantly localized on the F 2p AOs. These levels correspond to the valence σ and π orbitals of an F_6 cage. They are modified somewhat by bonding interactions with the Np valence AOs, notably the 6d contributions to the $1e_g$ and $1t_{2g}$ MOs and the 5f interactions in the $1t_{1u}$, $1t_{2u}$, and $2t_{1u}$ levels. This calculation suggests that metal−ligand covalent bonding is provided by a mixture of metal 6d and 5f AOs and that there is significant π interaction ($1t_{2g}$ and $1t_{2u}$), a result supported by previous work.[42]

Table 1. Nonrelativistic Molecular Orbital Energies and Mulliken Percent Compositions of the Valence Levels of NpF_6

molecular orbital	energy (eV)	% Np	% F	principal metal contributions
$2e_g$	+4.065	115.86	−15.86	115.86% 6d
$4t_{1u}$	+0.301	101.75	−1.75	101.75% 7p
$2t_{2g}$	−0.091	90.28	9.72	90.28% 6d
$2a_{1g}$	−0.446	103.90	−3.90	103.30% 7s
$3t_{1u}$	−7.037	65.34	34.66	59.38% 5f
$2t_{2u}$	−8.461	83.30	16.70	83.30% 5f
$1a_{2u}$ (HOMO)	−8.967	100.00	0.00	100.00% 5f
$2t_{1u}$	−10.887	28.60	71.40	15.96% 5f, 13.10% 6p
$1t_{1g}$	−11.490	0.00	100.00	
$1t_{2u}$	−12.398	16.80	83.20	16.80% 5f
$1a_{1g}$	−12.485	−3.82	103.82	
$1t_{1u}$	−12.919	27.05	72.95	23.74% 5f
$1t_{2g}$	−13.107	11.76	88.24	11.76% 6d
$1e_g$	−13.716	12.12	87.88	12.12% 6d

Table 2. Correlation between the Irreducible Representations of the Single Group O_h and Double Group O_h^*

O_h	O_h^*	O_h	O_h^*
a_{1g}	$e_{1/2}^+$	a_{1u}	$e_{1/2}^-$
a_{2g}	$e_{5/2}^+$	a_{2u}	$e_{5/2}^-$
e_g	$g_{3/2}^+$	e_u	$g_{3/2}^-$
t_{1g}	$g_{3/2}^+ + e_{1/2}^+$	t_{1u}	$g_{3/2}^- + e_{1/2}^-$
t_{2g}	$g_{3/2}^+ + e_{5/2}^+$	t_{2u}	$g_{3/2}^- + e_{5/2}^-$

Above the $2t_{1u}$ MO are the predominantly metal-localized levels. The 5f manifold comes first, with one electron in the $1a_{2u}$ highest occupied molecular orbital (HOMO). The $3t_{1u}$ MO has the greatest fluorine character and is destabilized above the other two 5f-based MOs, reflecting its significant metal−ligand σ^* antibonding nature. The remaining metal-localized orbitals (the $2a_{1g}$ MO and above) lie at significantly higher energy.

The bonding in UF_6^- and PaF_6^{2-} is similar to that described for NpF_6. A band of mainly fluorine-localized MOs is below the metal 5f manifold, which in turn is lower than the other metal-based MOs. The most interesting comparisons among the three systems relate to the metal contributions in the MOs. The metal 6d AO contribution to the $1e_g$ and the $1t_{2g}$ MOs is approximately the same in all three complexes (ca. 10−12%). In contrast, the 5f orbital character of the $1t_{1u}$, $1t_{2u}$, and $2t_{1u}$ MOs increases from PaF_6^{2-} to UF_6^- to NpF_6; for example, the 5f contribution in the $1t_{2u}$ MO increases from 6.0 to 11.3 to 16.8% from Pa to U to Np. Correspondingly, the f-orbital contribution to the $2t_{2u}$ and $3t_{1u}$ levels decreases as one progresses from Pa to U to Np (e.g. 5f character for the $2t_{2u}$ MO: PaF_6^{2-}, 94.1%; UF_6^-, 88.8%; NpF_6, 83.3%). These observations are consistent with stabilization of the metal 5f AOs from Pa to U to Np,[5,43,44] which fosters a stronger interaction with the F_6 cage orbitals.

Relativistic Calculations. There are two major consequences of relativity for the electronic structure of actinide systems. The first is the significant modification of the valence AO energies as a result of the stabilization of the inner core s and p electrons, which are moving at classical velocities that are appreciable fractions of the speed of light. The effect on the valence orbitals is to contract slightly the s and p levels and to destabilize the more diffuse d and f functions, which experience reduced nuclear charge due to increased shielding by the s and p electrons.[12]

The second consequence is the coupling of the electron's intrinsic spin angular momentum with that imposed by its orbital

(43) Desclaux, J.-P. *At. Data Nucl. Data Tables* **1973**, *12*, 312.
(44) Pyykkö, P.; Laaksonen, L. *J. Phys. Chem.* **1984**, *88*, 4892.

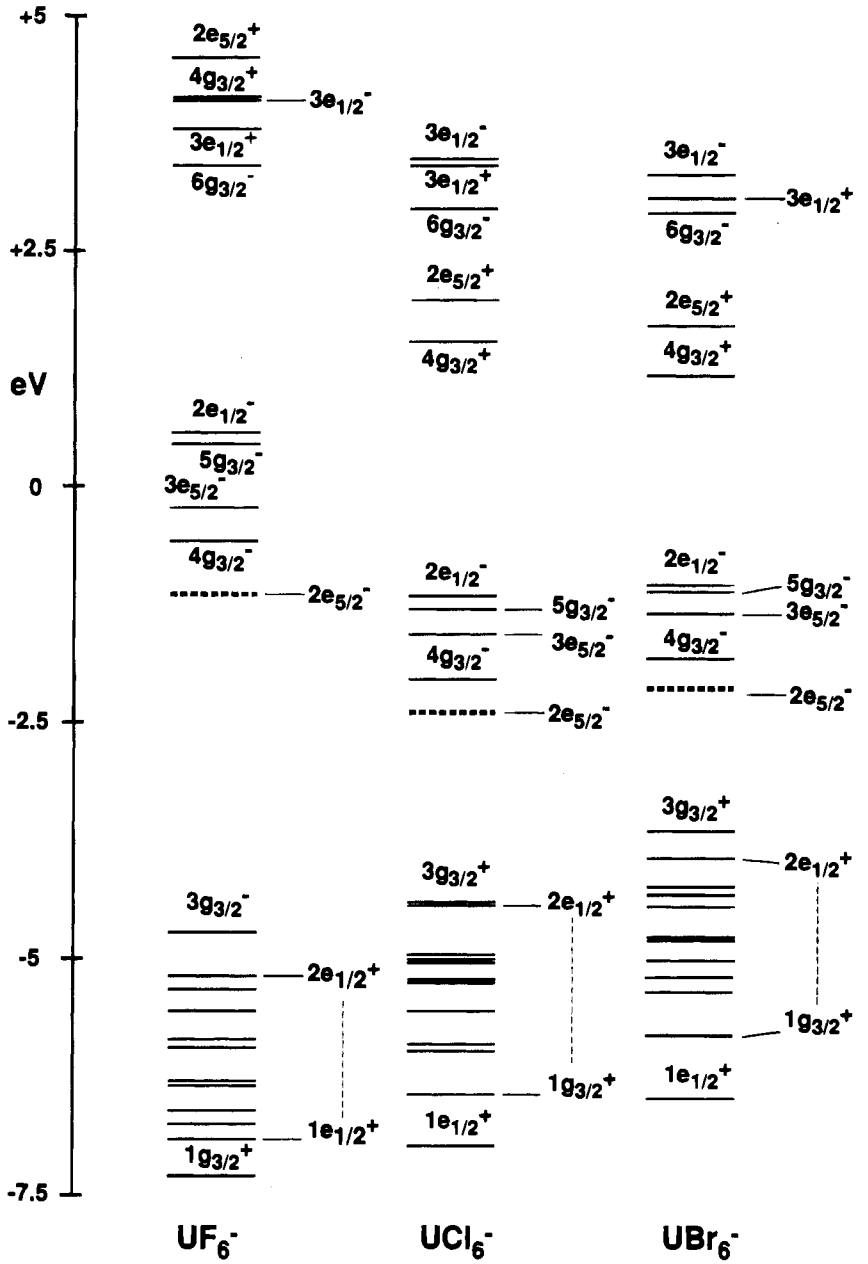

Figure 2. Molecular orbital energy level diagrams for UF_6^-, UCl_6^-, and UBr_6^-, calculated using the relativistic DV−Xα method. The highest occupied orbital is the $2e_{5/2}^-$ level in each case and is represented by a dashed line.

motion, an effect that is increasingly important for heavy-element systems. All electronic states in actinide complexes are therefore properly characterized by half-integral angular momentum values and must be described using double point group symmetry notation.[45] For the octahedral point group, the most significant effect of spin−orbit coupling is the lifting of the 3-fold degeneracy of the spatial t orbitals. The relationship between the spatial MOs of the O_h point group and the spin orbitals of the O_h^* double group is given in Table 2.

Figure 2 presents MO energy level diagrams for UF_6^-, UCl_6^-, and UBr_6^-, calculated using the relativistic DV−Xα method. The nonrelativistic and relativistic MO energies and percent compositions for UF_6^- are given in Table 3 and are representative of most of the calculations discussed here (*vide infra*). Figure 3 shows the energy levels of PaX_6^{2-} (X = F, Cl, Br, I), and the results for PaF_6^{2-}, UF_6^-, and NpF_6 are given in Figure 4.

(45) Salthouse, J. A.; Ware, M. J. *Point Group Character Tables and Related Data*; Cambridge University Press: London, 1972.

UF_6^-, UCl_6^-, and UBr_6^-. The relativistic calculation on UF_6^- (Figure 2) is in many ways similar to its nonrelativistic counterpart. Among the valence orbitals, the F 2p-based orbitals are at the most negative eigenvalues, followed by the U 5f manifold and a large energy gap to the remaining metal-localized MOs. Once again, the calculation predicts one electron in the lowest energy uranium-based orbital, the $2e_{5/2}^-$ HOMO. This is also true of UCl_6^- and UBr_6^-, the results on which are broadly similar to those on UF_6^-.

Numerous interesting trends are exhibited by the monoanionic uranium salts. Of the predominantly halogen-localized levels, there is a gradual destabilization as the ligand is changed from fluorine to chlorine to bromine. The orbitals that best illustrate this point are the $2e_{1/2}^+$ and $3g_{3/2}^+$, the relativistic equivalents of the $t_{1g}(\pi)$ set. In the nonrelativistic approach, these orbitals are restricted by symmetry to have no metal content. Although this symmetry constraint is lifted in O_h^*, the $2e_{1/2}^+$ and $3g_{3/2}^+$ orbitals contain virtually no metal character (cf. Table 3). Hence these orbitals reflect most closely the energy of the halogen *n*p

Table 3. Nonrelativistic and Relativistic Molecular Orbital Energies and Mulliken Percent Compositions of the Valence Levels of UF_6^-

Nonrelativistic

molecular orbital	energy (eV)	% U	% F	principal metal contributions
$2e_g$	+8.361	112.73	−12.73	112.73% 6d
$2t_{2g}$	+4.672	90.72	9.28	90.72% 6d
$2a_{1g}$	+3.952	104.71	−4.71	104.71% 7s
$4t_{1u}$	+3.920	101.61	−1.61	101.61% 7p
$3t_{1u}$	−1.382	75.44	24.56	75.44% 5f
$2t_{2u}$	−2.179	88.79	11.21	88.79% 5f
$1a_{2u}$ (HOMO)	−2.432	100.00	0.00	100.00% 5f
$2t_{1u}$	−4.549	18.06	81.94	8.13% 5f, 9.98% 6p
$1t_{1g}$	−5.180	0.00	100.00	
$1t_{2u}$	−5.773	11.29	88.71	17.29% 5f
$1t_{1u}$	−6.165	21.29	78.71	18.39% 5f
$1a_{1g}$	−6.250	−1.97	101.97	
$1t_{2g}$	−6.375	11.35	88.65	11.35% 6d
$1e_g$	−7.033	11.38	88.62	11.38% 6d

Relativistic

molecular orbital	energy (eV)	% U	% F	principal metal contributions[a]
$5g_{3/2}^+$	+7.317	112.76	−12.76	95.63% 6d, 17.13% 6$\bar{d}$
$2e_{5/2}^+$	+4.573	89.02	10.98	89.02% 6d
$4g_{3/2}^+$	+4.143	87.82	12.18	29.57% 6d, 58.25% 6$\bar{d}$
$4e_{1/2}^-$	+4.119	102.57	−2.57	102.57% 7$\bar{p}$
$3e_{1/2}^+$	+3.807	106.85	−6.85	106.85% 7s
$6g_{3/2}^-$	+3.422	100.91	−1.91	100.91% 7p
$3e_{1/2}^-$	+0.594	85.86	14.14	84.74% 5f
$5g_{3/2}^-$	+0.458	86.43	13.57	67.85% 5f, 15.73% 5$\bar{f}$
$3e_{5/2}^-$	−0.233	94.38	5.62	90.37% 5f, 4.01% 5$\bar{f}$
$4g_{3/2}^-$	−0.558	88.08	11.92	20.84% 5f, 66.67% 5$\bar{f}$
$2e_{5/2}^-$ (HOMO)	−1.141	96.20	3.80	6.16% 5f, 90.04% 5$\bar{f}$
$3g_{3/2}^-$	−4.721	12.96	87.04	7.54% 6p, 3.47% 5$\bar{f}$
$2e_{1/2}^+$	−5.191	0.00	100.00	
$3g_{3/2}^+$	−5.311	0.06	99.94	
$2e_{1/2}^-$	−5.563	5.07	94.93	4.45% 7$\bar{p}$
$1e_{5/2}^-$	−5.865	9.90	90.10	5.52% 5f, 4.35% 5$\bar{f}$
$2g_{3/2}^-$	−5.932	10.09	89.91	8.40% 5f
$1g_{3/2}^-$	−6.282	16.82	83.18	4.97% 5f, 9.23% 5$\bar{f}$
$1e_{1/2}^-$	−6.327	15.68	84.32	13.46% 5f
$1e_{5/2}^+$	−6.637	13.73	86.27	13.73% 6d
$2g_{3/2}^+$	−6.750	13.20	86.80	8.79% 6d, 4.41% 6$\bar{d}$
$1e_{1/2}^+$	−6.860	2.99	97.01	
$1g_{3/2}^+$	−7.266	13.82	86.18	7.25% 6d, 6.57% 6$\bar{d}$

[a] Unbarred labels refer to the higher angular momentum j-based atomic orbital; barred, to the lower.

valence AOs in the complex. The weighted average energy of the $2e_{1/2}^+$ and $3g_{3/2}^+$ MOs is −5.27 eV in UF_6^-, −4.42 eV in UCl_6^-, and −3.78 eV in UBr_6^-, in accord with the relative electronegativities of the halogens. Consistent with this observation, the energy gap between the halogen-based levels and the uranium 5f manifold decreases from UF_6^- to UBr_6^-. It is noticeable that while the $2e_{1/2}^+$ and $3g_{3/2}^+$ MOs are the least stable of the ligand levels in UCl_6^-, and UBr_6^-, the $3g_{3/2}^-$ orbital has a more positive eigenvalue in UF_6^-. This effect arises from interligand repulsions, which will be most significant in UF_6^- on account of the appreciably shorter halogen−halogen distances.

Inasmuch as the valence np AOs of the halogens rise in energy from fluorine to bromine, it is expected that they will come into closer energetic proximity with the metal orbitals, which may result in greater metal/ligand mixing. We can examine this effect by comparing the uranium 6d AO character of the $1g_{3/2}^+$, $2g_{3/2}^+$, and $1e_{5/2}^+$ MOs of the three complexes. These are the relativistic analogues of the $1e_g$ (metal−ligand $d\sigma$) and $1t_{2g}$ (metal−ligand $d\pi$) orbitals. The uranium 6d contribution of the $1g_{3/2}^+$ through $1e_{5/2}^+$ MOs increases from 13.6% per orbital[46] in UF_6^- to 18.9% in UCl_6^- and 21.3% in UBr_6^-. The variation in the uranium 5f/7p (there are small but nonzero 7p contributions to some of the levels) AO character in the halogen-based orbitals is much less pronounced, rising from 12.3% in UF_6^- to only 13.7% in UBr_6^-. The greater variation of the 6d contribution is a result of the greater radial extension of the uranium 6d AOs over the 5f, with the consequence that they are better able to take advantage of the closer energy match with the ligand orbitals at the longer bond lengths of the chloride and bromide.

We note a significant difference in the ordering of the metal-localized orbitals above the 5f manifold in UF_6^- relative to its heavier congeners. In UCl_6^- and UBr_6^-, the first levels above the 5f manifold are the $4g_{3/2}^+$ and $2e_{5/2}^+$ orbitals (the relativistic equivalents of the $2t_{2g}$ MOs), whereas these orbitals are destabilized above the 7p and 7s levels in UF_6^-. This effect can once again be traced to the electrostatic effects of the much tighter F_6 cage.

PaF_6^{2-}, $PaCl_6^{2-}$, $PaBr_6^{2-}$, and PaI_6^{2-}. Figure 3 presents the relativistic results for the PaX_6^{2-} systems. The results for $PaCl_6^{2-}$, $PaBr_6^{2-}$, and PaI_6^{2-} bear some similarities to the results for the UX_6^- systems. The energies of the halogen-based levels become more positive as the ligands become heavier, and there is a decreasing gap between ligand- and metal-localized orbitals. The protactinium 6d contribution to the $1g_{3/2}^+$ through $1e_{5/2}^+$ MOs increases from $PaCl_6^{2-}$ to PaI_6^{2-}, although the effect is not as significant as in UX_6^-.

It is clear from Figure 3 that the results for PaF_6^{2-} are somewhat different from those for the other PaX_6^{2-} systems and indeed for all of the other molecules in this study. All of the fluorine-based eigenvalues appear to lie approximately 1 eV too positive, on the basis of an extrapolation of the heavier halogen results and a comparison with the UX_6^- ions. Furthermore, while the 5f manifold is quite separate from both the ligand-localized MOs and the vacant metal orbitals in all seven of the other title systems, in PaF_6^{2-} the levels immediately above the $2e_{5/2}^-$ HOMO are mixtures of the Pa 5f and 7p AOs. This phenomenon will clearly affect the calculated absorption spectrum of PaF_6^{2-} in that our calculation indicates that the f → f transitions should be almost isoenergetic with the f → p transitions. The origin of this effect in PaF_6^{2-} remains as yet unclear. We feel that the results do not make sense from a chemical standpoint but note that a variety of different alterations to the computational input converge to essentially the same answers. We have included the PaF_6^{2-} results for consistency and completeness but wish to emphasize that they must be treated with some skepticism. We do not, however, believe that they detract from the excellent agreement between theory and experiment found for the other seven systems under investigation.

PaF_6^{2-}, UF_6^-, and NpF_6. Figure 4 compares the relativistic results for PaF_6^{2-}, UF_6^-, and NpF_6. The MOs of NpF_6 are similar to those of UF_6^- in their ordering, although a comparison of eigenvalues is not valid on account of the differing charges required to ensure that the molecules are isoelectronic. The metal 6d AO character of the $1g_{3/2}^+$ through $1e_{5/2}^+$ MOs is approximately constant, decreasing from 14.4% per orbital in NpF_6 to 12.4% in PaF_6^{2-}. There is a significant difference,

(46) In the calculation of these contributions, the total 6d AO character (6d + 6$\bar{d}$, where d refers to the higher angular momentum AO and $\bar{d}$ to the lower) has been summed over the MOs involved, weighted according to their number of Kramers degeneracies (i.e. 1 for $e_{5/2}^+$ and 2 for $g_{3/2}^+$). The result is then divided by the total number of Kramers degeneracies (in this case 5) to yield the contribution per orbital.

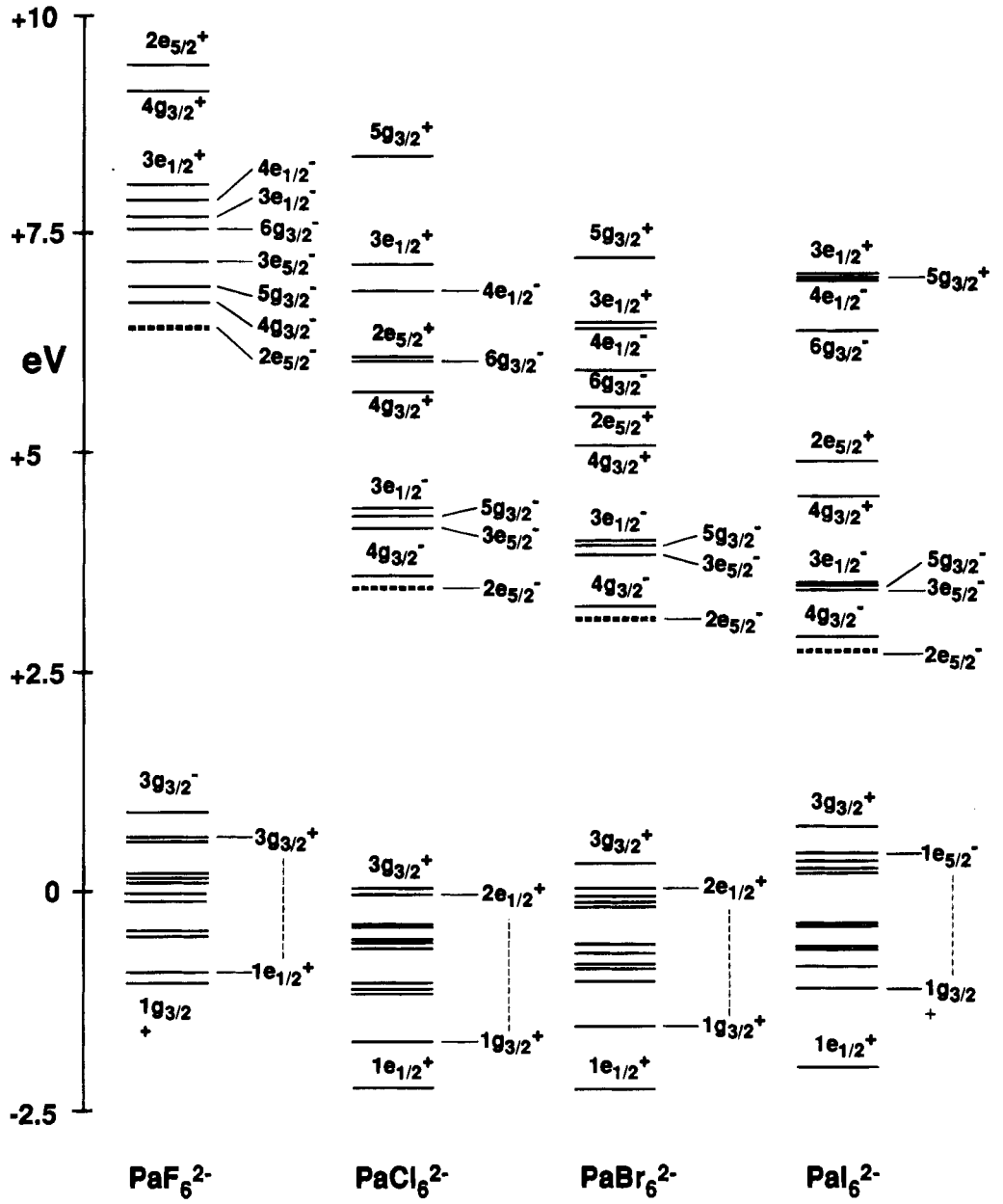

Figure 3. Molecular orbital energy level diagrams for PaF_6^{2-}, $PaCl_6^{2-}$, $PaBr_6^{2-}$, and PaI_6^{2-}, calculated using the relativistic DV−Xα method. The highest occupied orbital is the $2e_{5/2}^-$ level in each case and is represented by a dashed line.

however, in the metal 5f contributions to the fluorine-localized levels, falling from 17.9% per orbital in NpF_6 to 12.3% in UF_6^- to 8.2% in PaF_6^{2-}. The short M−F bond length in NpF_6 is a contributory factor, but possibly the main reason for the effect is the increase in the metal atom's formal charge from +4 in PaF_6^{2-} to +6 in NpF_6. As the formal charge increases, the 5f AOs are brought into significantly closer energetic proximity to the fluorine valence orbitals, an effect that is less pronounced for the 6d orbitals owing to the difference in primary quantum shell.

The Metal-Localized Electron. Before a discussion of the spectroscopic properties of the f^1 complexes, it is instructive to examine the nature of the highest-occupied electron in these complexes. In all cases, this unpaired electron is nearly entirely localized on the actinide center, as has been seen in earlier relativistic calculations.[40,41]

We can view the splitting of the f orbitals from two limiting cases, i.e. the ligand-field splitting and the spin−orbit splitting. Recall that, in the nonrelativistic case, the ligand field splits the 5f orbitals as $a_{2u} < t_{2u} < t_{1u}$. Table 2 shows the double-group representations generated by these representations of O_h. If ligand-field splitting is dominant, we therefore expect the double-group MOs to split as $e_{5/2}^- < (g_{3/2}^- + e_{5/2}^-) < g_{3/2}^- + e_{1/2}$).

We can refine this picture by considering the splitting of atomic 5f orbitals under the influence of spin−orbit effects. In a free metal atom or ion with a $5f^1$ configuration, spin−orbit coupling splits the f orbitals into a 6-fold degenerate ($j = {}^5/_2$, denoted $\bar{f}$) level below an 8-fold degenerate ($j = {}^7/_2$, denoted f) set. The octahedral ligand field splits the $\bar{f}$ manifold into an $e_{5/2}^-$ and a $g_{3/2}^-$ level, while the f block splits into $e_{5/2}^-$, $g_{3/2}^-$, and $e_{1/2}^-$ levels. The splitting pattern under the influences of both ligand-field and spin−orbit effects is diagrammed qualitatively in Figure 5. The lowest level should be an $e_{5/2}^-$ orbital that is derived primarily from the $\bar{f}$ manifold, although mixing of f manifold character is allowed by symmetry.

This splitting pattern is indeed preserved in the relativistic calculations presented here. In all cases, the HOMO is an $e_{5/2}^-$ orbital that is >92% localized on the actinide atom. In the PaX_6^{2-} and UX_6^- systems, the actinide character is >90% $5\bar{f}$.

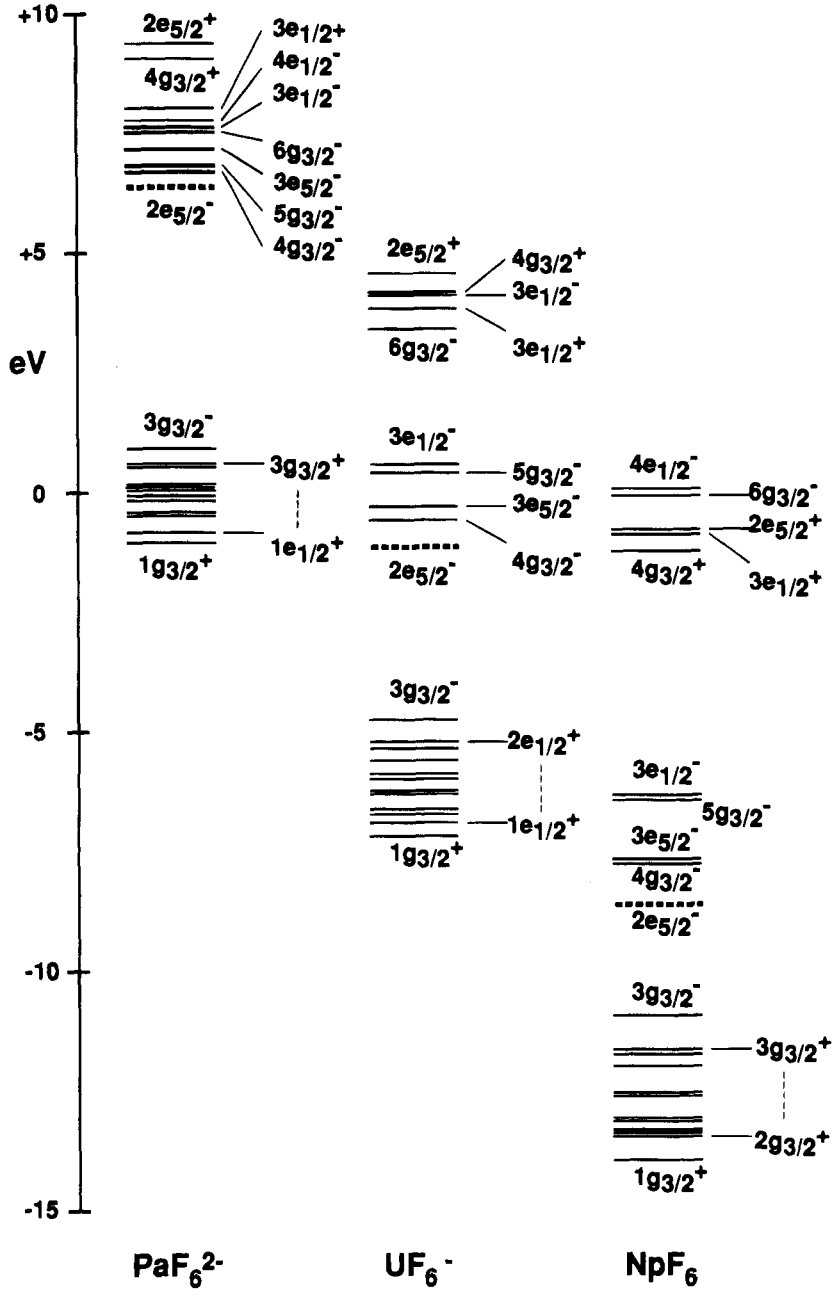

Figure 4. Molecular orbital energy level diagrams for PaF_6^{2-}, UF_6^-, and NpF_6, calculated using the relativistic DV−Xα method. The highest occupied orbital is the $2e_{5/2}^-$ level in each case and is represented by a dashed line.

Only in NpF_6 is there significant mixing of the $\bar{f}$ and f manifolds, as the HOMO is 84% $\bar{f}$ and 10% f in character. Notably, the orbital energies of the 5f-localized orbitals in NpF_6 exhibit a distinct "one-below-two-below-two" splitting pattern, characteristic of the ligand-field splitting (Figure 5). Hence, the increased ligand field and greater Np 5f/F 2p mixing in NpF_6 serve to alter the nature of the 5f-based orbital splitting pattern away from that expected of free Np^{6+}. The other complexes exhibit the "two-below-three" pattern that is indicative of dominance of the spin−orbit effects.

Optical Transition Energies. The electronic transitions that are observed in the absorption spectra of $5f^1$ AnX_6^{q-} systems can be divided into two general classes: transitions of the single metal-localized electron into vacant MOs also of predominant metal character and transitions of halogen-based electrons into these orbitals (charge-transfer transitions). The energies of these transitions, calculated using both nonrelativistic and relativistic approaches, are given for NpF_6 and UF_6^- in Tables 4 and 5, respectively. Table 6 presents the relativistic transition energies for UCl_6^-, UBr_6^-, $PaCl_6^{2-}$, $PaBr_6^{2-}$, PaI_6^{2-}, and PaF_6^{2-}. As discussed above, we believe that the results for the last ion are of dubious validity. In all cases, the experimental and, where available, previous theoretical data are provided.

While our calculations provide the energies of the possible electronic transitions, we have not made any attempt to predict their degree of "allowedness"; i.e., we have not calculated oscillator strengths. For the nonrelativistic and relativistic approaches alike, the symmetry requirement for an electronic transition to be permitted is that the direct product of the initial-state symmetry, the dipole moment operator, and the final-state symmetry contain the totally symmetric irreducible representation of the O_h (or O_h) point group.[47] Formally, therefore, many of the predicted transitions are forbidden, especially the f → f

(47) Cotton, F. A. *Chemical Application of Group Theory*, 3rd ed.; Wiley: New York, 1990.

Table 4. Nonrelativistic and Relativistic Electronic Transition Energies of NpF_6, Calculated by the Transition-State Method

Nonrelativistic

transition	associated state	transition type	calcd energy (cm^{-1})	transition	associated states	transition type	calcd energy (cm^{-1})
$1a_{2u} \rightarrow 2t_{2u}$	T_{2u}	Np 5f → 5f	4992	$2t_{1u} \rightarrow 1a_{2u}$	T_{1u}	F → Np CT	14331
$1a_{2u} \rightarrow 3t_{1u}$	T_{1u}	Np 5f → 5f	18413	$2t_{1u} \rightarrow 2t_{2u}$	$A_{1u} + E_u + T_{1u} + T_{2u}$	F → Np CT	16466
$1a_{2u} \rightarrow 2t_{2g}$	T_{2g}	Np 5f → 6d	76289	$2t_{1u} \rightarrow 3t_{1u}$	$A_{2u} + E_u + T_{1u} + T_{2u}$	F → Np CT	27366
				$1t_{1g} \rightarrow 1a_{2u}$	T_{1g}	F → Np CT	26406

Relativistic

transition	associated states	transition type	calcd energy (cm^{-1}) this work	calcd energy (cm^{-1}) Koelling et al.[a]	calcd energy (cm^{-1}) Kocab[b]	exptl energy (cm^{-1})[c]
$2e_{5/2}^- \rightarrow 4g_{3/2}^-$	$G_{3/2}^-$	Np $5\bar{f} \rightarrow 5\bar{f}/5f$	7018	8066[e]	7098	7610
$2e_{5/2}^- \rightarrow 3e_{5/2}^-$	$E_{5/2}^-$	Np $5\bar{f} \rightarrow 5f$	8762	9437	8146	9366
$2e_{5/2}^- \rightarrow 5g_{3/2}^-$	$G_{3/2}^-$	Np $5\bar{f} \rightarrow 5f/5\bar{f}$	18748	20728	18792	*d*
$2e_{5/2}^- \rightarrow 3e_{1/2}^-$	$E_{1/2}^-$	Np $5\bar{f} \rightarrow 5f$	21179	21777	19357	
$2e_{5/2}^- \rightarrow 4g_{3/2}^+$	$G_{3/2}^+$	Np $5\bar{f} \rightarrow 6\bar{d}/6d$	62671	58797[e]		
$3g_{3/2}^- \rightarrow 2e_{5/2}^-$		F → Np CT	22602			
$3g_{3/2}^- \rightarrow 4g_{3/2}^-$		F → Np CT	28029	27181		
$3g_{3/2}^- \rightarrow 3e_{5/2}^-$		F → Np CT	30599	28874		
$3g_{3/2}^- \rightarrow 5g_{3/2}^-$		F → Np CT	38446	39037		
$3g_{3/2}^- \rightarrow 3e_{1/2}^-$		F → Np CT	40959	40328		
$3g_{3/2}^+ \rightarrow 2e_{5/2}^-$		F → Np CT	31007	28552[e]		
$3g_{3/2}^+ \rightarrow 4g_{3/2}^-$		F → Np CT	36236	35327[e]		
$3g_{3/2}^+ \rightarrow 3e_{5/2}^-$		F → Np CT	38921	48474		

[a] Data from ref 41. [b] Data from ref 42. [c] Data from ref 28. [d] Subsequent peaks cannot justifiably be associated with individual electronic transitions. [e] Transition state calculates that were actually converged to self-consistency. Other values are taken from orbital energy differences in transition state calculations involving other orbitals with similar localization properties.

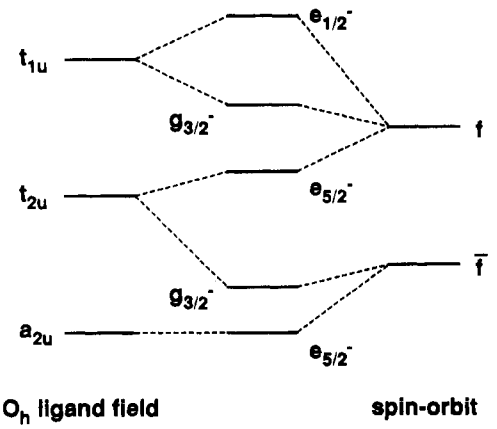

Figure 5. Qualitative correlation diagram showing the combined effects of ligand-field and spin–orbit splitting on the energies of 5f orbitals of the early actinide elements. The leftmost column shows the splitting of the f orbitals under an octahedral ligand field. The rightmost column shows the spin–orbit splitting of the atomic 5f orbitals into $j = {}^5/_2$ ($\bar{f}$) and $j = {}^7/_2$ (f) levels. The central column shows the correlation of these splittings; the labels shown are representations of the O_h^* double group.

transitions with which we are most concerned (the label "f → f" refers to the predominant AO character of the MOs involved in the transition). These transitions are often observed experimentally as very weak (or sometimes nonexistent) components of a band system arising from excitation of vibrational modes, which couple to the electronic transition to lift the symmetry restrictions. Other transitions are permitted in their own right, and consequently f → d and certain charge-transfer bands will have much greater oscillator strengths and may well obscure the weaker f → f peaks should they occur in the same energy range.

We shall consider NpF_6 first. The nonrelativistic calculation on the molecule indicates that the single electron in the $1a_{2u}$ HOMO can undergo two f → f transitions, to the $2t_{2u}$ and $3t_{1u}$ MOs. The $1a_{2u} \rightarrow 2t_{2u}$ transition is predicted at 4992 cm^{-1}, with the $1a_{2u} \rightarrow 3t_{1u}$ at substantially higher energy (18 413 cm^{-1}). The lowest allowed f → d transition ($1a_{2u} \rightarrow 2t_{2g}$) is predicted to occur at much higher energy (76 289 cm^{-1}). By contrast, the charge-transfer transitions are predicted to begin at only 14 331 cm^{-1} ($2t_{1u} \rightarrow 1a_{2u}$). Consequently, the nonrelativistic calculation suggests that the $1a_{2u} \rightarrow 2t_{2u}$ f → f band would be masked by the onset of an entire series of ligand-to-metal charge-transfer transitions. The relatively low energy of these charge-transfer bands is a consequence of the energetic proximity of the neptunium 5f and fluorine 2p AOs.

It is unlikely that all of the charge-transfer transitions would be individually resolved in an absorption spectrum. Not only do most of them give rise to a number of distinct electronic states (Table 4), but the creation of holes in degenerate MOs and the single occupancy of previously unfilled degenerate levels are expected to produce substantial Jahn–Teller progressions.[26]

Turning now to the relativistic results, the most obvious difference is the prediction of four f → f transitions: spin–orbit coupling has lifted the degeneracies of the nonrelativistic

Table 5. Nonrelativistic and Relativistic Electronic Transition Energies of UF_6^-, Calculated by the Transition-State Method

Nonrelativistic

transition	associated states	transition type	calcd energy (cm^{-1})
$1a_{2u} \rightarrow 2t_{2u}$	T_{2u}	U 5f → 5f	2807
$1a_{2u} \rightarrow 3t_{1u}$	T_{1u}	U 5f → 5f	10929
$1a_{2u} \rightarrow 4t_{1u}$	T_{1u}	U 5f → 7p	59709
$2t_{1u} \rightarrow 1a_{2u}$	T_{1u}	F → U CT	21847

Relativistic

transition	associated states	transition type	calcd energy (cm^{-1})	exptl energy (cm^{-1})[a]
$2e_{5/2}^- \rightarrow 4g_{3/2}^-$	$G_{3/2}^-$	U $5\bar{f} \rightarrow 5\bar{f}/5f$	5085	
$2e_{5/2}^- \rightarrow 3e_{5/2}^-$	$E_{5/2}^-$	U $5\bar{f} \rightarrow 5f$	7392	7413
$2e_{5/2}^- \rightarrow 5g_{3/2}^-$	$G_{3/2}^-$	U $5\bar{f} \rightarrow 5f/5\bar{f}$	13968	13715
$2e_{5/2}^- \rightarrow 3e_{1/2}^-$	$E_{1/2}^-$	U $5\bar{f} \rightarrow 5f$	16013	15900
$2e_{5/2}^- \rightarrow 6g_{3/2}^-$	$G_{3/2}^-$	U $5\bar{f} \rightarrow 7p$	47458	
$3g_{3/2}^- \rightarrow 2e_{5/2}^-$	$G_{3/2}^-$	F → U CT	35497	

[a] Data from ref 29.

Table 6. Relativistic Electronic Transition Energies of UCl_6^-, UBr_6^-, $PaCl_6^{2-}$, $PaBr_6^{2-}$, PaI_6^{2-}, and PaF_6^{2-}, Calculated by the Transition-State Method

ion	transition	transition type	calcd energy (cm^{-1})	exptl energy (cm^{-1})
UCl_6^- [a]	$2e_{5/2}^- \rightarrow 4g_{3/2}^-$	U $5\bar{f} \rightarrow 5\bar{f}/5f$	3117	
	$2e_{5/2}^- \rightarrow 3e_{5/2}^-$	U $5\bar{f} \rightarrow 5f$	6688	6801
	$2e_{5/2}^- \rightarrow 5g_{3/2}^-$	U $5\bar{f} \rightarrow 5f$	9510	10190
	$2e_{5/2}^- \rightarrow 3e_{1/2}^-$	U $5\bar{f} \rightarrow 5f$	11340	11470
	$2e_{5/2}^- \rightarrow 4g_{3/2}^+$	U $5\bar{f} \rightarrow 6\bar{d}/6d$	35147	
	$3g_{3/2}^+ \rightarrow 2e_{5/2}^-$	Cl $\rightarrow$ U CT	21709	
UBr_6^- [b]	$2e_{5/2}^- \rightarrow 4g_{3/2}^-$	U $5\bar{f} \rightarrow 5\bar{f}/5f$	2774	
	$2e_{5/2}^- \rightarrow 3e_{5/2}^-$	U $5\bar{f} \rightarrow 5f$	6557	6823
	$2e_{5/2}^- \rightarrow 5g_{3/2}^-$	U $5\bar{f} \rightarrow 5f$	8749	9620
	$2e_{5/2}^- \rightarrow 3e_{1/2}^-$	U $5\bar{f} \rightarrow 5f$	10516	10555
	$2e_{5/2}^- \rightarrow 4g_{3/2}^+$	U $5\bar{f} \rightarrow 6\bar{d}/6d$	30646	
	$3g_{3/2}^+ \rightarrow 2e_{5/2}^-$	Br $\rightarrow$ U CT	17191	
$PaCl_6^{2-}$ [c]	$2e_{5/2}^- \rightarrow 4g_{3/2}^-$	Pa $5\bar{f} \rightarrow 5\bar{f}$	1724	2108
	$2e_{5/2}^- \rightarrow 3e_{5/2}^-$	Pa $5\bar{f} \rightarrow 5f$	5683	5250
	$2e_{5/2}^- \rightarrow 5g_{3/2}^-$	Pa $5\bar{f} \rightarrow 5f$	7219	7272
	$2e_{5/2}^- \rightarrow 3e_{1/2}^-$	Pa $5\bar{f} \rightarrow 5f$	8923	8173
	$2e_{5/2}^- \rightarrow 4g_{3/2}^+$	Pa $5\bar{f} \rightarrow 6\bar{d}/6d$	23541	20780, 20860[d]
	$3g_{3/2}^+ \rightarrow 2e_{5/2}^-$	Cl $\rightarrow$ Pa CT	39705	
$PaBr_6^{2-}$ [e]	$2e_{5/2}^- \rightarrow 4g_{3/2}^-$	Pa $5\bar{f} \rightarrow 5\bar{f}$	1415	
	$2e_{5/2}^- \rightarrow 3e_{5/2}^-$	Pa $5\bar{f} \rightarrow 5f$	5668	5365
	$2e_{5/2}^- \rightarrow 5g_{3/2}^-$	Pa $5\bar{f} \rightarrow 5f$	6766	6828
	$2e_{5/2}^- \rightarrow 3e_{1/2}^-$	Pa $5\bar{f} \rightarrow 5f$	8869	7480
	$2e_{5/2}^- \rightarrow 4g_{3/2}^+$	Pa $5\bar{f} \rightarrow 6\bar{d}/6d$	20817	19280[f]
	$3g_{3/2}^+ \rightarrow 2e_{5/2}^-$	Br $\rightarrow$ Pa CT	33864	
PaI_6^{2-} [g]	$2e_{5/2}^- \rightarrow 4g_{3/2}^-$	Pa $5\bar{f} \rightarrow 5\bar{f}$	1316	
	$2e_{5/2}^- \rightarrow 3e_{5/2}^-$	Pa $5\bar{f} \rightarrow 5f$	5627	5391
	$2e_{5/2}^- \rightarrow 5g_{3/2}^-$	Pa $5\bar{f} \rightarrow 5f$	6444	6506
	$2e_{5/2}^- \rightarrow 3e_{1/2}^-$	Pa $5\bar{f} \rightarrow 5f$	8413	6998
	$2e_{5/2}^- \rightarrow 4g_{3/2}^+$	Pa $5\bar{f} \rightarrow 6\bar{d}/6d$	18182	
	$3g_{3/2}^+ \rightarrow 2e_{5/2}^-$	I $\rightarrow$ Pa CT	25099	
PaF_6^{2-} [h]	$2e_{5/2}^- \rightarrow 4g_{3/2}^-$	Pa $5\bar{f} \rightarrow 5\bar{f}/5f$	3511	
	$2e_{5/2}^- \rightarrow 3e_{5/2}^-$	Pa $5\bar{f} \rightarrow 5f$	5954	5698
	$2e_{5/2}^- \rightarrow 5g_{3/2}^-$	Pa $5\bar{f} \rightarrow 5f/5\bar{f}$	10094	9708
	$2e_{5/2}^- \rightarrow 3e_{1/2}^-$	Pa $5\bar{f} \rightarrow 5f$	12245	11446

[a] Experimental data from ref 29; measured as $[(C_2H_5)_4N][UCl_6]$. [b] Experimental data from ref 29; measured as $[(C_2H_5)_4N][UBr_6]$. [c] Except as indicated, experimental data from ref 36; measured as $PaCl_6^{2-}$ doped in Cs_2ZrCl_6. [d] Experimental data from ref 33; measured as CH_3CN solutions of Cs_2PaCl_6 and $(NEt_4)_2PaCl_6$. [e] Except as indicated, experimental data from ref 31; measured as $[(C_2H_5)_4N]_2[PaBr_6]$. [f] Experimental data from ref 33; measured as CH_3CN solution of $(NEt_4)_2PaBr_6$. [g] Experimental data from ref 32; measured as $[(C_2H_5)_4N]_2[PaI_6]$. [h] Experimental data from ref 32; measured as $[(C_2H_5)_4N]_2[PaF_6]$.

t orbitals (for simplicity, when discussing transition types, we will group both $\bar{f}$ and f relativistic AOs under the label f unless specified otherwise, and similarly for the other relativistic AOs). The charge-transfer transitions are no longer predicted to mask the more energetic of the f $\rightarrow$ f shifts, as the least energetic $3g_{3/2}^- \rightarrow 2e_{5/2}^-$ charge-transfer transition does not occur until 22 602 cm^{-1}. This result is due to the destabilization of the neptunium 5f AOs relative to the fluorine 2p orbitals upon the incorporation of relativistic effects. Once again, the energy of the first f $\rightarrow$ d transition is very much higher than that of the f $\rightarrow$ f and charge-transfer transitions.

A comparison of our theoretical results with the available experimental data is enlightening. The energies of the two lower-energy f $\rightarrow$ f transitions of NpF_6 have been measured very precisely by Mulford et al.[20] and are found to lie at 7610 and 9366 cm^{-1}, respectively (Table 4). Our nonrelativistic calculation predicts only one band in the low-energy range, which is ca. 2600 cm^{-1} away from the first experimental peak. Thus the nonrelativistic calculation does a poor job of reproducing experiment, both qualitatively and quantitatively.

The relativistic approach fares much better, with both the calculated $2e_{5/2}^- \rightarrow 4g_{3/2}^-$ and $2e_{5/2}^- \rightarrow 3e_{5/2}^-$ transitions lying only ca. 600 cm^{-1} lower than the experimental values. The two previous theoretical studies—those of Koelling et al.[41] and Kocab[42]—enjoy a similar degree of success in quantitatively matching the matrix-isolated experimental spectrum. It is interesting to note that the investigation by Koelling et al. employed methodology very similar to ours. Their results are in slightly better agreement with the experimental values than are ours, which is puzzling in view of the fact that the self-consistent charge (SCC) charge-density fitting procedure that they used is more approximate than the SCM procedure that we used.

For the higher energy transitions we must rely on the lower resolution gas-phase spectra of Eisenstein and Pryce[26] and Steindler and Gerding.[27] This correlation is inconclusive, however, in that there are no well-defined f $\rightarrow$ f transitions above 10 000 cm^{-1}. At just above 17 000 cm^{-1}, a significant and constant signal occurs until 22 000 cm^{-1}, which sees the onset of a very intense, broad band with gentle maxima at ca. 39 000 cm^{-1} and 45 000 cm^{-1}. A number of small shoulders on the main peak occur over the energy range 22 000−28 000 cm^{-1}, but these cannot be justifiably ascribed to well-defined electronic absorptions. Although it is certainly possible that f $\rightarrow$ f transitions occur in this wavenumber range, there is no means by which they can be assigned with confidence to features in the experimental spectrum.

All three calculations predict the remaining two f $\rightarrow$ f transitions to lie in the approximate energy range 18 000−21 000 cm^{-1}. The energies of the charge-transfer transitions calculated by Koelling et al.[41] are close to our calculations, although they do not report what is possibly the most important one, namely $3g_{3/2}^- \rightarrow 2e_{5/2}^-$. Nevertheless, the two calculations are in agreement in predicting that the higher-energy f $\rightarrow$ f transitions be observed at an energy below the onset of the charge-transfer bands. This prediction is at odds with the experimental data, which give no clear indication of f $\rightarrow$ f transitions before the beginning of the very intense charge-transfer band.

We shall now consider the UX_6^- systems. The nonrelativistic and relativistic results for UF_6^- are presented in Table 5. The two f $\rightarrow$ f transitions predicted by the nonrelativistic calculation on UF_6^- are at significantly lower energies than the corresponding bands in NpF_6, reflecting the smaller ligand-field splittings in the uranium system. The first charge-transfer transition is predicted at 21 847 cm^{-1}, greater than that for NpF_6 on account of the larger energy difference between the uranium 5f and fluorine 2p AOs. The lowest energy non-f $\rightarrow$ f metal-localized transition is predicted to occur at high energy, 59 709 cm^{-1}, and it is 5f $\rightarrow$ 7p rather than 5f $\rightarrow$ 6d as is the case for NpF_6.

The relativistic calculation on UF_6^- displays features and trends similar to those discussed for NpF_6. Four f $\rightarrow$ f bands are expected, and the first charge-transfer transition is now predicted at 35 497 cm^{-1}, some 20 000 cm^{-1} removed from f $\rightarrow$ f. The $2e_{5/2}^- \rightarrow 6g_{3/2}^-$ (5f $\rightarrow$ 7p) transition is calculated to lie at 47 458 cm^{-1}. Once again, there are major differences in the number and energies of the electronic transitions predicted by the nonrelativistic and relativistic calculations.

Both calculations predict that the f $\rightarrow$ f spectrum should be free of charge-transfer transitions, a significant difference with

respect to NpF_6. This prediction is consistent with the experimental spectrum of $[Ph_4As^+][UF_6^-]$ reported by Ryan.[29] The spectrum exhibits three of the four expected f → f bands. The calculated energies of these bands are in excellent agreement with the experimental energies, as each of the three calculated values is within 253 cm^{-1} of the experimental value. The author notes that the lowest energy transition ($2e_{5/2}^- \rightarrow 4g_{3/2}^-$) is not observed because it lies at an energy below 5000 cm^{-1}, which was the low-energy limit of the spectrum. In an earlier experimental study, Reisfeld and Crosby found the lowest energy transition to be at ca. 4600 cm^{-1}.[48] Our calculated energy for this transition, 5085 cm^{-1}, is very close to this experimental limit and is also in good accord with the value (5400 cm^{-1}) calculated by Hay et al. using ab initio methods.[38] No experimental data are available above ca. 17 000 cm^{-1}, so it is not possible to compare the calculated charge-transfer onset with experiment.

The calculated transition energies of UCl_6^- and UBr_6^- (Table 6) are analogous to those of UF_6^-. For both ions, the lowest energy transition is $2e_{5/2}^- \rightarrow 4g_{3/2}^-$, which is not observed experimentally. The agreement between theory and experiment for the remaning f → f bands is only slightly less impressive than that found for UF_6^- and is generally excellent. Note that the transition energies in the UX_6^- systems generally decrease from X = F to Cl to Br, which reflects the smaller ligand-field splittings induced at greater M−X bond lengths.

In general, therefore, the optical spectroscopy of UF_6^-, UCl_6^-, and UBr_6^- is less uncertain than that of NpF_6. The f → f transitions are predicted and found to lie in an energy range uncluttered by charge-transfer shifts or other metal-localized transitions.

For the PaX_6^{2-} systems (X = Cl, Br, I), the calculations predict a very low energy (<2000 cm^{-1}) f → f band followed by a gap to the remaining f → f transitions, which lie between ca. 5500 and 9000 cm^{-1}. The first transition, $2e_{5/2}^- \rightarrow 4g_{3/2}^-$, corresponds to redistribution of the $5f^1$ electron with the f manifold, while the other three involve promotion to the f set of orbitals. The energies of all four of the excited levels of the $5f^1$ configuration have been determined experimentally for $PaCl_6^{2-}$, and it can be seen (Table 6) that the agreement between calculated and experimental data is very good. The $2e_{5/2}^- \rightarrow 3e_{1/2}^-$ transition is overestimated by some 750 cm^{-1}, an observation that is repeated in $PaBr_6^{2-}$ and PaI_6^{2-}. The agreement for the $2e_{5/2}^- \rightarrow 3e_{5/2}^-$ and $2e_{5/2}^- \rightarrow 5g_{3/2}^-$ transitions is rather better in all cases. As with the UX_6^- systems, the f → f transitions are predicted to be free from overlap with charge-transfer transitions.

Edelstein and co-workers recently provided several spectroscopic studies of the energies of the f → d transitions in PaX_6^{2-} systems.[33,34,36] We have calculated the energy of the first transition from the 5f to the 6d manifold for these systems. The room-temperature CH_3CN solution spectra of two different salts of $PaCl_6^{2-}$ show the lowest energy transition at ca. 20 800 cm^{-1}; our calculation overestimates the energy of this transition by some 3000 cm^{-1}. For $PaBr_6^{2-}$, we calculate the lowest energy f → d transition to occur at 20 800 cm^{-1}. This calculated value is in excellent accord with the transition energy observed in solution (19 280 cm^{-1}) and in dilute crystals of Pa^{4+} doped into suitable hosts (20 710 cm^{-1}).

(48) Reisfeld, M. J.; Crosby, G. A. *Inorg. Chem.* **1965**, *4*, 65.

Table 6 also presents the calculated and experimental energies for the f → f transitions of PaF_6^{2-}. As with the ground-state results, these data are included for completeness and should not have too much weight attached to them. It proved impossible to converge transition state calculations in which the orbital to which promotion was occurring was 7p localized, although the f → f transitions converted rapidly to give energies quite close to the experimental results. It would therefore seem that the problems associated with the PaF_6^{2-} calculations do not have a marked adverse effect on the calculated f → f transition energies.

Summary and Conclusions

The ground-state calculations on UF_6^-, UCl_6^-, and UBr_6^- indicate that metal−ligand covalent bonding is achieved through a mixture of metal 6d and 5f AO contributions. The latter is found to be approximately constant in all three molecules, while the 6d character of the predominantly halogen-localized orbitals increases significantly from UF_6^- to UBr_6^-. The 6d contribution to the $1t_{2g}$ (and relativistic equivalents) and the 5f character of the $1t_{2u}$ MOs suggests a not insignificant degree of metal−ligand π bonding.

A similar trend is observed in $PaCl_6^{2-}$, $PaBr_6^{2-}$, and PaI_6^{2-}, although the 6d:5f ratio does not increase from chloride to iodide to the same extent as in UX_6^-. The relativistic calculation on PaF_6^{2-} yields results that do not fit in with the trends in either UX_6^- or the heavier protactinium halides and must be treated with some caution.

The stabilization of the metal 5f AOs with respect to the other metal valence orbitals and the halogen *n*p AOs on moving from PaX_6^{2-} through UX_6^- to NpF_6 results in a significantly greater metal 5f contribution to the halogen-based MOs in NpF_6 than in any other molecule studied. Furthermore it alters the type of electronic transition that occurs in the energy range covered by optical spectroscopy. Ligand-to-metal charge-transfer transitions are predicted to occur at relatively low energies, owing to the energetic proximity of the neptunium 5f and fluorine 2p AOs. This is observed experimentally, although calculation and experiment differ in that the more energetic f → f transitions are predicted to come before the onset of the charge-transfer bands, which is not found to be the case.

For UX_6^-, the calculations predict f → f spectra that are energetically isolated from charge-transfer bands and 5f-to-other-metal-valence AO transitions. The quantitative agreement between relativistic theory and experiment is very good in all cases. This is also true of PaX_6^{2-} (X = Cl−I).

For all of the molecules studied, the relativistic calculations are much more successful than their nonrelativistic counterparts at reproducing experiment, both qualitatively and quantitatively. The generally excellent agreement between theory and experiment for the electronic transition energies of these hexahalides provides much justification and encouragement for similar calculations on more complicated $5f^1$ systems.

Acknowledgment. N.K. wishes to thank the Graduate School of The Ohio State University and the Science and Engineering Research Council (U.K.) for Postdoctoral Fellowships. We gratefully acknowledge support for this research from the Division of Chemical Sciences, U.S. Department of Energy (Grant DE-FG02-86ER13529), and from The Ohio Supercomputer Center.

IC950192C